energies

MDPI

Article

Investigating the Performance Capability of a Lithium-ion Battery System When Powering Future Pulsed Loads

Luke Farrier * and Richard Bucknall

Mechanical Engineering, University College London, London, WC1E 7JE, UK; r.bucknall@ucl.ac.uk

* Correspondence: luke.farrier.14@ucl.ac.uk

Received: 10 December 2019; Accepted: 8 March 2020; Published: 14 March 2020

Abstract: The supply of pulsed power loads is considered a key driver for the integration of energy storage systems (ESSs) with warship power systems. ESSs are identified as a means to offer fast response dynamics capable of driving pulsed loads for sustained periods. This paper contributes a novel investigation into the performance of a Nickel Manganese Cobalt based lithium-ion battery system to supply laser directed energy weapon (LDEW) loads for future warship combat power systems using time-domain simulation methodology. The approach describes a second order Thévenin equivalent circuit battery model validated against a battery module of a type used in commercial marine ESS. The ability of the battery system to power LDEW loads peaking at 2 MW for up to periods of four minutes were simulated for beginning of life (BoL) and degraded conditions. The repeatability of the pulsed power supply with ESS is also reported. Simulation results show that Quality of Power Supply (QPS) is maintained within acceptable transient tolerance using a feed-forward control circuit that controls the DC-DC converter interface between the battery system and the LDEW load. The results of the study demonstrate the battery system operating envelope for the LDEW under investigation.

Keywords: battery systems; equivalent circuit model; power quality

1. Introduction

Future warships are predicted to employ advanced weapon systems, the power for which will be drawn from the ships electric power system. Key among these advanced systems are high power laser directed energy weapons (LDEWs) characterized by a pulsed power profile [1–4]. Pulsed power load supply is an important factor driving change in power system design and is considered a primary requirement for the integration of energy storage devices that have fast response dynamics capable of driving pulsed loads for sustained periods [5]. At present, lower power LDEWs below 100 kW are being tested onboard warship power systems [6]. However, the peak pulse power requirement of LDEW systems is currently expected to be up to 2 MW [1–3,7].

Warships with an Integrated Power System may have large gas turbine generators with sufficient ramp rate capability to power megawatt level laser loads. However, this is not necessarily the case for ships with inherently reduced power generation capacity, such as ships with a hybrid electric and mechanical propulsion system [1]. This is because it is unknown whether smaller generator sets, characteristic of hybrid propulsion systems, can provide the intake of combustion air and fuel flow rates to meet the ramp rate demand of high power LDEW loads. Hence there is a need to investigate appropriate energy storage systems (ESSs) that can facilitate LDEW pulsed power loads for use on warships with hybrid power and propulsion systems.

If the time duration required to charge the intermediate store between the ships generators and the pulsed load is critical, then power density of the energy store has priority over energy density. Such a

system may be very high power, single shot capable (e.g., electromagnetic railgun or aircraft launch), where the energy store has sufficient capacity for one shot before recharging is required, leading to a capacitor being more suitable than batteries [8]. However, if the time to recharge is less critical, the power and energy balance of lithium-ion (li-ion) batteries may be more suitable. This power and energy balance is an important characteristic of ESSs to power future LDEW loads. ESSs are required to facilitate up to 4 min of LDEW operation [9]. Using a battery ESS to power the LDEW for 4 min, instead of intermittently pulsing a high power capable capacitive energy store, alleviates the recharging transients that would otherwise be transmitted to the ships generators.

A review of the literature highlighted a gap in the understanding of the capability of batteries when used in pulse power applications. Publications on batteries used to power pulsed loads are few [2,10,11] and includes the authors' own publications [12,13]. Simulation-based work in [2] has demonstrated that lithium iron phosphate (LFP)-based li-ion batteries could be capable of providing for such loads. However, the li-ion battery model, power electronic interface and control system in [2] were not presented in sufficient detail to conclude the battery performance limitations under LDEW operation. The authors in [2] suggested that the interface between the battery and LDEW does however, require close attention due to the sensitivity of LDEWs to power quality. Furthermore, compliance of the LDEW with Quality of Power Supply (QPS) standards ensures system integrity when considering wider system integration and the correct operation of equipment that may be connected to a DC bus where the LDEW is located.

The work in [10] detailed the design and development of a hybrid ESS approach to power railgun load profiles. Here an LFP based battery charges a capacitive pulsed power circuit at 12 kJ/s to 5 kV in 5 s before a single shot is taken. While the on-time of 5 s, is of comparable duration with anticipated LDEW loads [1,2] the capacitor load off-time, from the perspective of the battery, is 10 ms as the shot is taken. The work of [11] focused on power hardware in the loop testing of a 1000 V, 660 kW, 200 MJ li-ion battery. One of their aims was to present results of the commissioning and testing of the battery when supplying periodic and stochastic pulsating loads. The battery system was subjected to two-level periodic 1 kA load pulses. The authors in [11] did not discuss the limitations of this loading on the operating envelope of the battery. Instead, their work contributed to the de-risking effort of integrating ESSs with warship power systems to supply pulsed loads. In [2,10,11], the discussion of the DC/DC converter control system to manage the pulsed power load was not included in the work.

Previous work in [12] by the authors, presented the parameterization of a cell equivalent circuit simulation model, and validation of the cell simulation model against charge and discharge profiles. The work in [12] also designed the DC/DC control system and presented system response to a 2 MW, 100 ms rise time LDEW load when the battery commences discharge at 90% state of charge (SoC). This work was expanded upon in [13], where the SoC window of the battery when powering 2 MW, 1.75 MW and 1.5 MW LDEW loads with 100 ms rise time at beginning of life (BoL) conditions was defined, the thermal losses of the system under LDEW operation were also presented. In this paper, additional modelling beyond [12,13] has been done, to advance knowledge of battery performance when powering laser pulsed loads.

This paper contributes further knowledge on the performance of batteries for laser pulsed load application in a typical warship power system arrangement in the following four ways. First, the Nickel Manganese Cobalt (NMC) battery cell model developed in [12], is validated at battery module level at the ampere discharge rates required to power an LDEW. This substantiates the fidelity of the battery model parameterized previously in [12]. Second, additional results beyond [12,13] have been obtained and are presented, which define the BoL battery operational envelope against the 4-min LDEW operation target [9]. Analysis of the ability of a li-ion battery ESS to achieve the 4-min LDEW operation target has been absent from the literature. The third contribution is analysis of the system QPS performance against design criteria [14] with respect to the rise times of the LDEW load when supplied by the li-ion NMC based battery system. Fourth, the degraded performance of the battery as a consequence of cyclic aging is presented to fully define the battery system operating

envelope under LDEW loading. Contribution one has been experimentally validated. Experimental verification of the remaining contributions is in the scope of future work. The consequences of degraded performance of li-ion NMC based battery systems on LDEW operation have were not reported in [2,10,11]. The significance of the work in this paper is to suggest that batteries can be used successfully in laser pulse load applications in warships.

The paper is organized as follows. Section 2 introduces the battery based pulsed power model, control system design and verification, and battery model validation at module level. The BoL performance of this system is evaluated in Section 3 to define the operating envelope of the battery system for varying LDEW load powers, rise times and battery state of charge (SoC). The ability of the battery system to repeat the pulsed load supply is also discussed. Section 4 considers how the system operates in degraded states as a consequence of aging. Section 5 concludes the findings of this paper.

2. System Overview

The simplified equivalent circuit of the battery based pulsed power system modelled in this work is presented in Figure 1. The LDEW pulsed load only operates under battery power, therefore the system in Figure 1 is disconnected from the ship distribution system during firing and reconnected during the recharging phase of the ensuing LDEW operation. This pulsed load operating principle is similarly adopted in [2,8]. Isolation during LDEW operation prevents potential excessive voltage and frequency perturbations on the main bus that would be experienced under LDEW operation that are outside operating limits [1].

Efforts to develop pulsed laser systems for warship application have concentrated on three types of electrically powered lasers; slab solid-state, fiber solid-state, and free electron lasers (FELs) [7,15]. The solid state lasers (SSLs) are of interest for medium power (<600 kW optical power [3]), and FEL for high power lasers in the multi-MW range [15]. The type of LDEW focused upon here is the slab SSL due to its relative technological maturity compared to FELs. In high-powered slab SSLs, such as those in [1,3], hundreds of laser diodes are combined to form an array [15,16]. The equivalent circuit of a laser diode can be represented by a parallel RLC circuit as described by [17], which is dominated by the diode differential resistance. Therefore, the LDEW is modelled as a variable resistance, as shown in Figure 1.

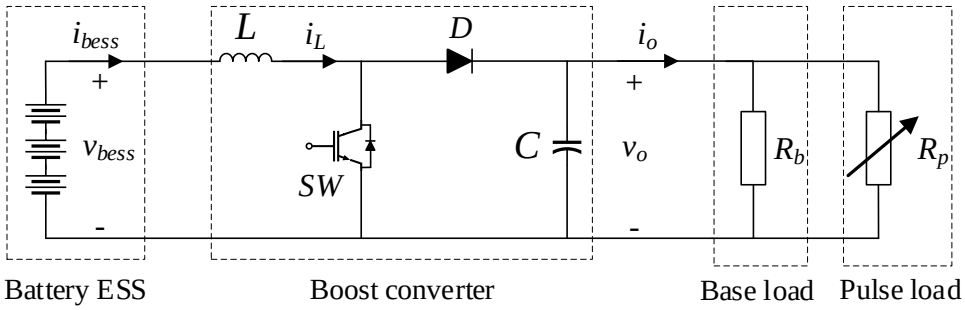

Figure 1. Simplified equivalent circuit of the simulated system.

2.1. Battery Model

The battery model represents four parallel strings, each consisting of twenty-two series connected modules with li-ion polymer pouch type cells. The battery cell cathode material is lithium nickel manganese cobalt and the anode is graphite. The module and string characteristics are summarized in Table 1. Four strings is the minimum required to satisfy the LDEW load demands as previously demonstrated in [13]. The battery string specification in Table 1 is representative of the Orca system from Corvus Energy, each string being rated at 125 kWh.

Table 1. Battery module and string specification.

Parameter	Module	String	Unit
Nominal capacity	128	128	Ah
Peak voltage	50	1100	V
Nominal voltage	45	980	V
Cut-off voltage	36	800	V
Peak cont. discharge current	768	768	A
Peak charge current	384	384	A
Cells	24 (12s2p)	528	

A second order behavioral Thévenin equivalent circuit of a cell is scaled in series and parallel to represent the four parallel string battery system. The cell equivalent circuit is shown in Figure 2. The equivalent circuit parameters were extracted through analysis of experimental voltage and current time-series data from pulsed discharge current pulse test data, described in previous work [12]. The method followed is a fast, analytical method that negates the need for iterative simulations to optimize the parameters. Further detail on the time-domain model and equivalent circuit parameterization procedure followed can be found in [12,18] respectively. An overview of alternative parameterization procedures can be found in [19,20]. For brevity, the model used in this work is summarized mathematically by (1) and (2).

$$v_t = v_{OCV}(SoC) - R_0 i_t - v_1(SoC) - v_2(SoC) \tag{1}$$

$$\begin{bmatrix} \dot{v_1} \\ \dot{v_2} \\ \dot{SoC} \end{bmatrix} = \begin{bmatrix} -1/R_1C_1 & 0 & 0 \\ 0 & -1/R_2C_2 & 0 \\ 0 & 0 & 0 \end{bmatrix} \begin{bmatrix} v_1 \\ v_2 \\ SoC \end{bmatrix} + \begin{bmatrix} 1/C_1 \\ 1/C_2 \\ 1/Q \end{bmatrix} i_t \tag{2}$$

where v_t is the terminal voltage, v_{OCV} is the open circuit voltage, R_0 is the equivalent series resistance, i_t is the terminal current, SoC and Q are the battery SoC and capacity respectively. The transient circuit voltages are donated by v_1 and v_2 , with associated non-linear complex impedance RC pairs.

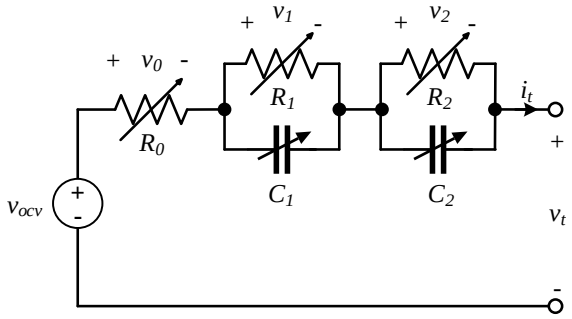

Figure 2. Second order Thévenin equivalent circuit used to represent li-ion polymer cell.

For higher fidelity modelling of the battery system, the cells could be modeled separately [21], however separate modelling of 2112 cells was deemed inappropriate due to the substantial computational complexity. Aggregating the cell model in series and parallel allows effects such as cell voltage variation and thermal imbalance to be omitted [22]. To evaluate the loss of fidelity from this modeling decision, module level validation was conducted.

2.2. Battery Module Validation

The battery model was validated at module level by aggregating the cell to a 12 series and 2 parallel (12s2p) arrangement and applying experimental current profiles with a peak current discharge

rate of 2 C and 4.5 C. These rates are representative of the discharge currents required from the battery system to meet the power levels of the LDEW loads under investigation.

The results of module level validation are shown in Figure 3 and summarized in Table 2. For both cases, experimental current data was inputted to the model and the voltage response of the battery then recorded. The root mean square percentage error (RMSPE) and mean absolute percentage error (APE) of the module voltage were then determined using (3) and (4) respectively.

$$RMSPE = 100\sqrt{\sum_{i=1}^{n}\left(\frac{v_{mod}-\hat{v}_{mod}}{\hat{v}_{mod}}\right)^2\frac{1}{n}} \tag{3}$$

$$Mean\ APE = \frac{100}{n}\sum_{i=1}^{n}\left|\frac{v_{mod}-\hat{v}_{mod}}{\hat{v}_{mod}}\right| \tag{4}$$

where $\hat{v}_{mod}$ are the measured values and v_{mod} is the simulated module voltage, and n is the number of validation measurement instances. All measurements were sampled at 1 Hz.

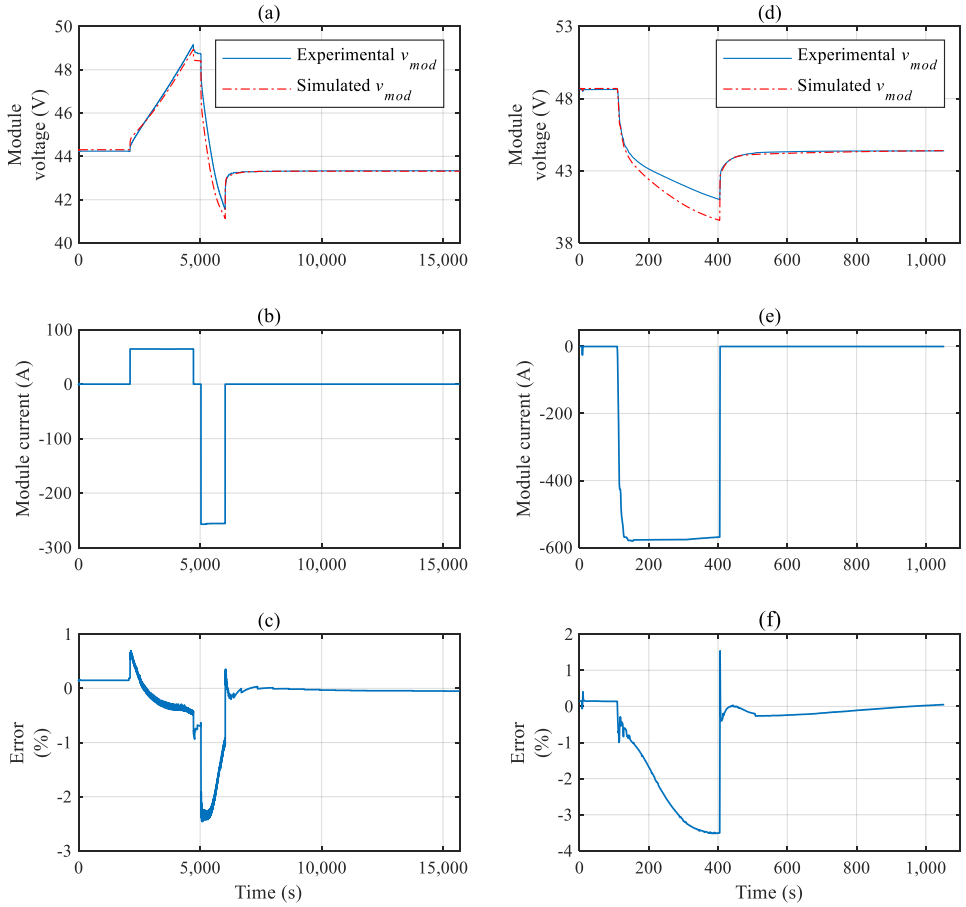

Figure 3. Module (**a**) voltage validation response (**b**) 1C charge/2.5C discharge profile (**c**) developed error and (**d**) voltage validation response (**e**) 4C discharge profile (**f**) developed error.

Table 2. Battery module validation results summary.

Experiment	Max APE	Mean APE	RMSPE
Module 2 C discharge	2.53%	0.23%	0.17%
Module 4.5 C discharge	3.51%	0.76%	0.72%

The validation results in Figure 3a,d show good correlation with experimental results. The voltage errors (Figure 3c,f) are a product of the model parameters being based on 0.5 C pulsed discharge experimental data, compared to the higher discharge rates used for validation. Moreover, the cell model is isothermal. Noise in the error signal is attributed to the sampling frequency of 0.2 Hz in the experimental data. In summary, 3.5% is the maximum validation error (Table 2), and this is deemed low enough to consider the battery model as sufficiently validated for time-domain simulation.

2.3. Laser Directed Energy Weapon Load

The LDEW characteristics modeled are applicable to SSL weapons, where the power demand characteristics used are based on [1,3], and summarized in Table 3. The peak LDEW power of 2 MW represents the worst case expected peak power requirement from [1,3], which is commensurate with demands for future naval ships. As the laser diode equivalent circuit is dominated by the diode differential resistance, the LDEW is modeled as a variable resistor, R_P, to aggregate the behavior of the pulse load and reduce computational complexity. This was deemed acceptable as similar studies such as [23,24], have modelled the pulsed load as a controlled current source.

Table 3. Laser directed energy weapon (LDEW) load characteristics examined.

Parameter	Value	Unit
LDEW power demand after losses	2.0, 1.75, 1.5	MW
LDEW peak current	1.33, 1.17, 1.00	kA
LDEW bus voltage	1500	V
Rise time/fall time, T_r	100, 50, 25	ms
Pulse duration, T_P	2.5	s
Duty cycle	40	%
Base load	50	kW

There is an inherent delay to the full radiant intensity of the laser aperture of SSLs, which is in the tens of milliseconds [25]. This delay is captured in the model as the rise and fall time of the LDEW load, which is varied from 25 to 100 ms as part of Study 1 in Section 3. The pulse duration, T_P of the LDEW load is 2.5 s, as used in [1]. This concurs with T_P that are in the order of seconds [15,16]. R_P is controlled to achieve a trapezoidal pulse defined by the rise/fall times, pulse duration and LDEW power as described in Table 3.

2.4. DC/DC Converter and Control System Design

The DC/DC converter is required to control the output power on the DC bus to produce a load profile of trapezoidal shape that is required by the pulsed load. Further, the converter is required to ensure QPS to the load, which is very important for LDEW systems as discussed in [2]. The single stage unidirectional DC/DC boost converter, shown in Figure 1, was selected for this work as the voltage transformation ratio is compatible with the battery ESS and LDEW. Isolated DC/DC converters such as a full bridge converter could be more suitable if there was a larger voltage ratio. However, isolation converters could decrease the power density of the system due to the increased quantity of semiconductor devices and high frequency transformer.

The DC/DC converter in Figure 1 utilizes a cascaded PI control structure as depicted in Figure 4. The outer loop regulates the output voltage v_O and sets the command for the inner loop controller that is responsible for controlling the input inductor current i_L subject to the maximum battery current i_{bmax}. The output of the inner loop controller is the duty cycle D, which governs the PWM switching signals that drive the IGBT switching devices. The feedforward controller, $G_{\text{ff}}(s)$ uses the relation

described by (5) to handle the abrupt LDEW load variation and corresponding voltage drop caused by the current drawn across the battery system's internal resistance.

$$G_{\mathrm{ff}}(s) = \frac{i_o v_o^*}{v_{bess}} \tag{5}$$

where i_o and v_o^* are the converter output current and voltage reference respectively, and v_{bess} is the battery system voltage. This can similarly be applied to compensate supercapacitor stacks that exhibit wide voltage variation during discharge [26].

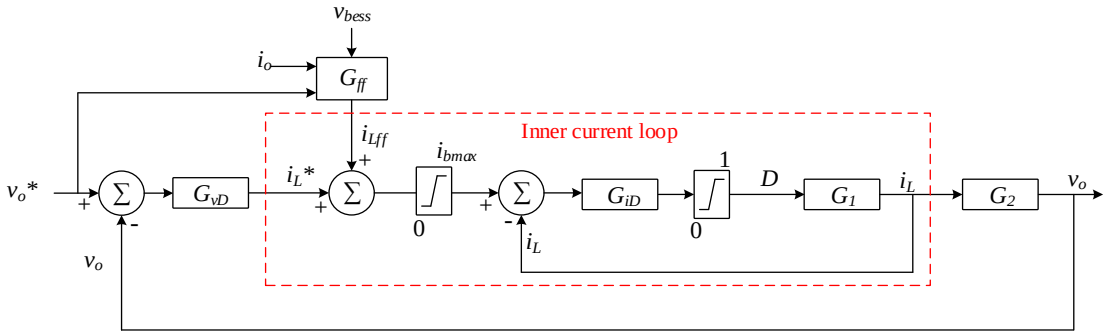

Figure 4. Schematic of DC/DC boost converter cascaded control configuration with feedforward loop.

The input inductor was selected to attenuate 4% switching ripple at peak pulse load, without limiting the pulse rise time to less than 25 ms (see Table 3). The output capacitance was specified to maintain v_o to within ±1% ripple at peak pulse power. The converter and control system parameters are specified in Table 4. The outer loop controller was designed to have 1/5th the bandwidth of the inner to prevent mutual coupling of the controllers. The corresponding unit step response for the inner and outer loop closed loop transfer functions is shown in Figure 5. The response in Figure 5 verifies that the control system met the rise time requirement of the LDEW load. The outer loop response showed a 5% overshoot and the presence of the Right-Hand Plane (RHP) zero as there was a phase delay in the response, inherent with boost converter control. This was mitigated by the inclusion of the feedforward control loop.

Table 4. DC/DC converter parameters.

Parameter	Value	Unit
Input inductor, L	780	µH
Output voltage, v_o	1.5	kV
Output capacitor, C	5	mF
Battery C-rate limit, i_{bmax}	3	kA
PWM switching frequency	5	kHz
Inner loop proportional gain, K_p	0.00029	
Inner loop integral gain, K_i	0.285	
Outer loop proportional gain, K_{p2}	0.09	
Outer loop integral gain, K_{i2}	10	

Figure 6 provides a performance comparison of the controller with and without feedforward loop control against recommended practice for voltage quality [14]. Comparison of Figure 6a,b shows that despite providing the pulse power required, the output voltage dipped to 24% below rated voltage when the pulse rose, and peaked at 52% above rated voltage when the pulse unloaded; both peaks being outside acceptable limits. Conversely, the feedforward loop maintained the voltage within ±0.5%, which was within the 10% tolerance prescribed by [14]. The impact of the feedforward controller was a small overshoot at the leading edge of the output power response shown in Figure 6d.

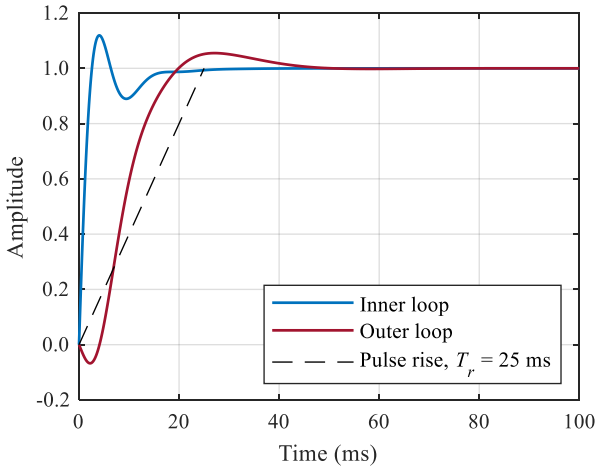

Figure 5. Unit step response of the inner and outer closed loop transfer functions of the DC/DC boost converter control system.

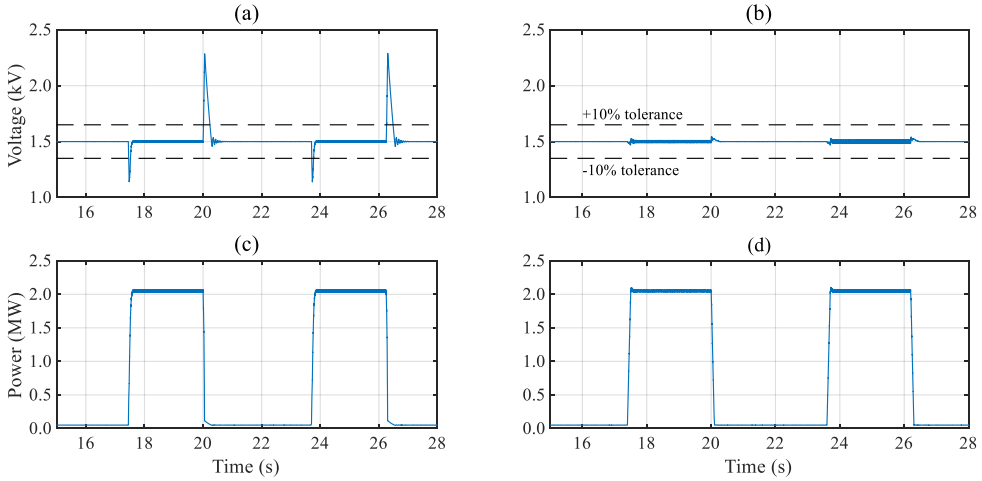

Figure 6. Output voltage and power response to 2 MW LDEW pulse with 100 ms rise time (**a**,**c**) without, and (**b**,**d**) with feedforward controller respectively.

2.5. Study Limitation

Robust thermal management is required for battery systems to remove heat generated by the exothermic reaction in the cells and ensure that the body temperature of the cells in battery modules does not exceed 65 °C [10]. The development of a thermal model for the simulated battery system in this paper is planned for future work. The thermal implications are that as the temperature of the cells rises with continued LDEW loading, the cell internal resistance would decrease and therefore the magnitude of the voltage drop due to the load would be reduced. The addition of a thermal model could increase the duration of actual LDEW operation compared to the method used in this work.

3. Study 1: Beginning of Life System Results

The first study assessed the BoL performance of the battery based pulsed power system presented in Figure 1 for the LDEW parameters detailed in Table 3. For each LDEW load, simulations were conducted at 10% intervals between 90% and 50% SoC, for 100 ms, 50 ms and 25 ms pulse rise times. LDEW loading commenced at 5 s to allow the system to attain steady state. Each simulation was prescribed to terminate if either the 800 V battery cut-off, 3072 A discharge current, 20% SoC or 10 min simulation limit were surpassed. The battery was limited to operate between 90% and 20% SoC to limit cell degradation [22].

3.1. System Response

The system response to a 2 MW LDEW load with 25 ms rise time is presented in Figure 7, showing the first 60 s of operation. The system response to a 2 MW LDEW load with 100 ms rise time is presented in [12]. For this case, the 800 V cut-off limit was breached at 407 s (65 shots). The final recorded SoC for the case in Figure 7 was 68%. Whilst cut-off voltage is often interpreted as an indication of low SoC, the cut-off voltage termination criteria was used as a protection measure to reduce the risk of degradation mechanisms such as lithium plating. Lithium plating could cause power and capacity fade of the battery system through loss of lithium or active material at the cell anode [27].

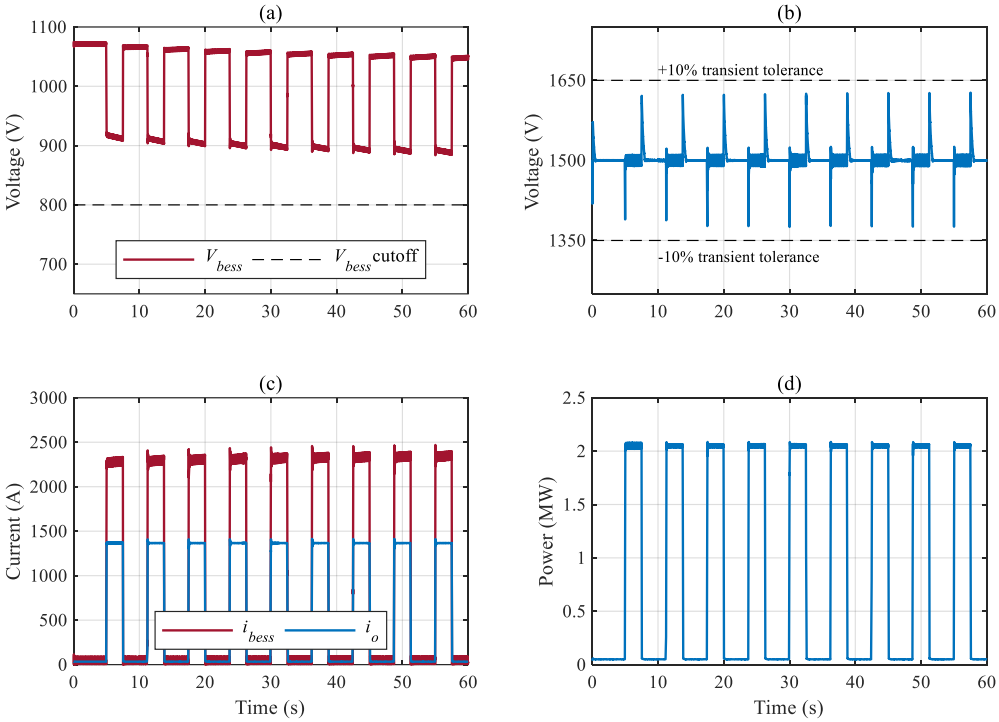

Figure 7. Simulated (**a**) battery voltage (**b**) converter output voltage, v_o (**c**) current and (**d**) LDEW power response when the battery commences 2 MW, 25 ms rise time LDEW pulse load at 40% duty cycle at 90% SoC.

Figure 7a shows that under the 2 MW pulse there was a large voltage drop across the battery system terminals, which was primarily a function of the battery cell internal resistances (~0.8 mΩ). The fast rise and fall times of the load were the cause of the transients. The frequent pulsing characteristic of the LDEW could be perceived as a short circuit. However, the short circuit current of the load was 2.68 kA, whilst the peak load current was 1.33 kA. In a short circuit event, depending on SoC, the battery will either trip on overcurrent, which is above the 3 kA discharge limit or under voltage protection, which is the cut-off voltage of the battery ESS.

With reference to the circuit diagram in Figure 1, v_o on the LDEW bus was maintained within transient limits as shown in Figure 7b. The largest dip and overshoot in voltage were triggered by the fast rise and fall time of the LDEW pulse respectively. Throughout the simulation, i_{bess} was maintained below the 3072 A limit as shown in Figure 7c.

3.2. Quality of Power Supply

Figure 8 shows that under each LDEW and di/dt condition, v_o was maintained within the transient voltage limits except for the 2 MW, 25 ms rise time case, which exceeded the 10% maximum tolerance which corresponds to the battery unloading during the LDEW load fall time. With increasing LDEW

load and pulse rise time the transient response of v_o increased. There was a noteworthy delta between the 25 ms when compared with the 50 ms and 100 ms rise times for the 2 MW load. The large di/dt for the 2 MW, 25 ms rise time case is attributed to the control system dynamics at the rising and falling edges of the LDEW pulse. The control system was slower to track the step change in load current fed forward to the inner control loop (Figure 4), therefore the deviation magnitude of v_o under the fast rise times was of higher magnitude than the 50 ms and 100 ms cases.

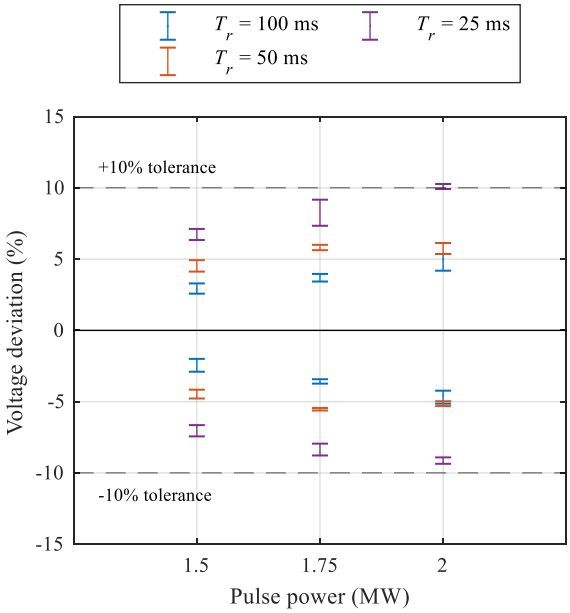

Figure 8. Maximum voltage deviation on the output LDEW bus showing upper and lower bounds of voltage deviation for Study 1.

3.3. Battery Operating Envelope

Figure 9 shows how the battery performed against the four-minute operation target with varying SoC and pulse rise time. Figure 9 expands on the results previously produced in [13] for T_r = 100 ms only. For the 2 MW LDEW load, the initial SoC of the battery is required to be 81% and 83% for the short rise time and long rise time respectively (Figure 9a). Conversely as shown in Figure 9b the 1.75 MW LDEW requires a minimum SoC of between 65%–66%. Figure 9b further demonstrates that the pulse rise time does not have a dramatic impact on the operating window of the battery for the 1.75 MW load case.

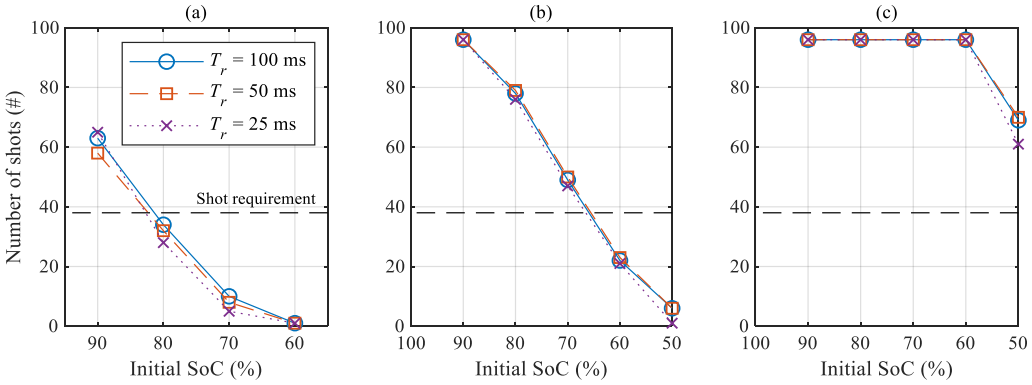

Figure 9. Battery shot performance against pulse rise time and sustained four minute operation target for (**a**) 2 MW (**b**) 1.75 MW and (**c**) 1.5 MW LDEW load.

The high di/dt loading for the 2 MW, 25 ms case causes the cut-off voltage to be exceeded sooner, this is associated with the previously discussed control system dynamics. The 1.5 MW LDEW load case meets the target for all SoC above 45% SoC at BoL.

3.4. Repeatability of LDEW Power Supply

Following a single LDEW engagement, if there is an operational need for a second subsequent engagement, then the battery ESS needs to be recharged at its maximum charge rate to ensure LDEW availability. The maximum charging current allowed by the cells in the battery system is 1536 A. The duration to recharge depends on the potential required operating time of the LDEW in the second engagement and initial SoC at the beginning of the first engagement. For the purpose of this analysis, the operating time of the second engagement is assumed equal to the 4-min requirement specified by [9]. Figure 10a shows the final SoC after the first engagement, and Figure 10b shows the recharge time required for the ships' generators to provide power to recharge the battery ESS to the minimum initial SoC that would allow a second engagement. If the initial SoC of the first engagement is greater than 55% and 78% for the 1.5 MW and 1.75 MW respectively, a second engagement could be possible immediately following the first.

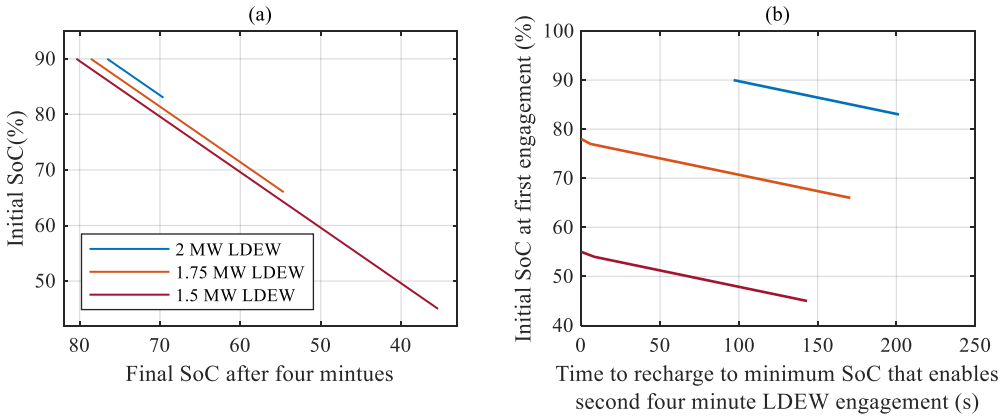

Figure 10. Battery ESS (**a**) final SoC after four minute engagement and (**b**) recharge time to minimum SoC at maximum charging current of 1536 A.

The 2 MW LDEW case in Figure 10b shows that if the initial SoC at the first engagement was 83%, a recharge time of 201 s was required to facilitate a second engagement. Conversely, the minimum recharge time to operate the 2 MW LDEW was 97 s. The charging current rate of the li-ion cell with NMC chemistry was limited to avoid fast charging problems such as lithium plating and SEI layer breakdown [27,28]. Alternative materials such as carbon-coated niobium titanate oxide (TNO) have been identified as important for improving fast recharge rates of cells in the future [29]. Batteries with a TNO anode with NMC cathode at 49 Ah capacity, were demonstrated by [30] to fast charge from 0% to 90% SoC in less than 6 min, comparatively the NMC chemistry used here took 13 min.

4. Study 2: Degraded Performance Results

The aim of this study was to assess the performance envelope of the battery system following illustrative degradation. This was conducted by simulating the system following the equivalent of 500 cycle intervals using resistance increase and capacity fade data from the extensive degradation study presented in [31,32] for a 4.2 V NMC based li-ion pouch cell rated at 20 Ah nominal capacity. The study in [31,32] is a good benchmark from which to formulate a comparison for degraded performance. It is noted the cells in this work were of larger capacity at 64 Ah. The parameters interpreted from the results of their work used in this investigation are shown in Table 5 for cells that were cycled to 20% SoC at 25 °C.

Table 5. Degraded battery performance test matrix based on [31,32].

Condition	Internal Resistance Increase (%)	Capacity Decrease (%)	Cycles at 80% DOD (#)
1	1	2.5	500
2	1.5	4.5	1000
3	7	6	1500
4	16	8	2000
5	19	10	2500

The system in Figure 1 was simulated with 25 ms rise time for each of the degraded conditions in Table 5 to determine how the battery SoC operating envelope for the LDEW diminishes with cyclic aging. This was conducted by incrementing the initial SoC, running the simulation and then evaluating whether the 4-minute target was achieved before either of the cut-off, current limit, or SoC termination criteria in Section 3 were met. It should be noted that the cell degradation modes influence the characteristics of the cell open circuit voltage (OCV), depending on whether a loss of lithium inventory, or loss of active material of the anode or cathode has occurred [27]. For the purpose of this investigation it has been assumed that the nominal OCV between 90% and 20% SoC was not affected by the degradation modes. Detailed information on how degradation modes affect the OCV can be found in [27].

Figure 11 illustrates how cyclic ageing conditions could affect the useable SoC range that is capable of achieving the four minute LDEW operation target. The large internal resistance increase at condition 3 notably reduced the useable SoC window, predominantly for conditions 4 and 5. This is a consequence of the voltage drop increase due to the increased internal resistance with degradation compared to the BoL capacity. From BoL to condition 5 for the 2 MW LDEW, the SoC window reduced from 7% below 90% SoC, to 2.3% below 90% SoC.

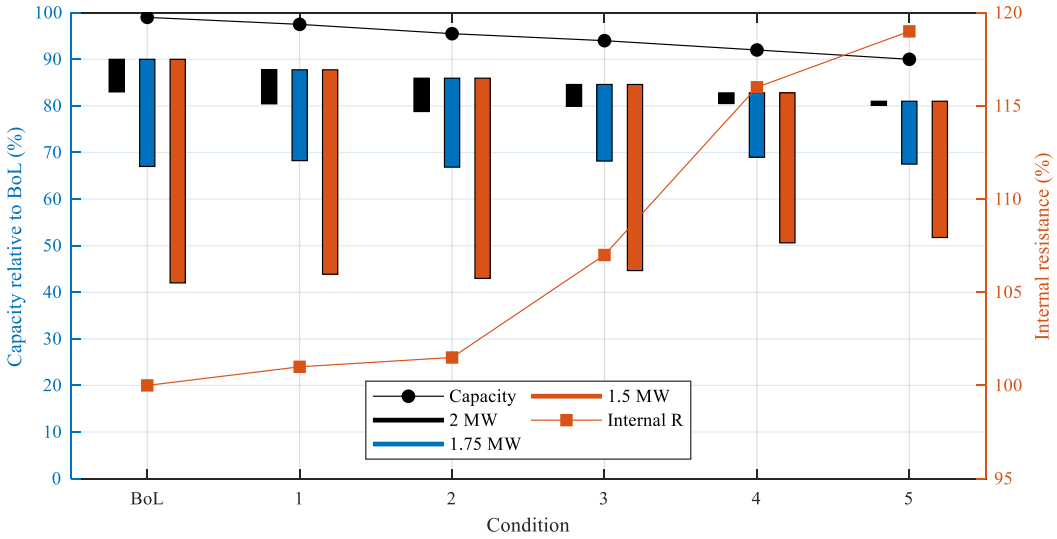

Figure 11. Battery system operating envelope with degradation condition and LDEW power to meet LDEW operational requirement of four minutes. The 2 MW, 1.75 MW and 1.5 MW results pertain to the capacity on the left-y axis.

Despite the capacity reducing by 10% and resistance increase of 19% compared to BoL, the results indicate that the LDEW at each pulse power was still capable of meeting the 4-min target, however this would require a robust energy management system to ensure the battery system SoC remains within the specified range of Figure 11 at commencement of LDEW operation. Alternatively, power generation sources in the ship power system may need to contribute to a proportion of LDEW demand.

The control system performance and QPS response of the system as the battery system degraded was insignificant when compared to the BoL results in Section 3. The maximum transient voltage

deviation for the 2 MW, 1.75 MW and 1.5 MW were +0.5%, +0.7% and +0.6% respectively above the mean BoL performance reported in Figure 8. The most significant impact the degraded system would have is on the operating envelope of the battery and thermal management system from the cell exothermic reaction under LDEW loading.

5. Conclusions

The impact of this work is upon the design of future laser pulsed load systems. This paper has produced the first set of results to define the operating envelope of a li-ion NMC based battery system when powering laser pulsed loads in warships and has included two key studies. These studies have clearly identified the following aspects associated with the design and operation; QPS, battery operating envelope under BoL and degraded conditions, and repeatability of pulsed load supply.

The control system for the DC-DC boost converter with a load and battery voltage feedforward term was verified and demonstrated the mitigation of system voltage transients for the majority of simulation conditions tested. Using the proposed feedforward loop, the QPS response reduced the voltage deviation magnitude by up to 51.5% when the battery unloads following a 2 MW LDEW pulse compared to without the feedforward loop. Using the proposed system, the voltage was maintained within recommended QPS practice for DC loads. The rise time of the 2 MW LDEW load should be greater than 25 ms, shorter rise times could cause departure from the recognized limits of standard IEEE 1709 [14], triggering protection relays of other equipment.

This work demonstrated that the NMC based li-ion system simulated is theoretically capable of supplying large LDEW loads for sustained periods, subject to the SoC window at commencement of operation, the limits for which were highlighted in this paper for BoL and degraded conditions. The 2 MW LDEW load has significant consequences for the useable SoC range of the battery ESS. At a best case, the initial SoC range is 7% of useable capacity due to the short rise time and magnitude of the LDEW load.

The repeatability limits of the pulsed load supply with the battery were demonstrated. A benefit of this, is that the ship operator is provided with knowledge regarding the capability of the battery to supply LDEW loads based upon the battery system initial SoC.

The work presented in this paper paves the way for further studies into the thermal modelling of the battery system and practical testing of battery systems powering laser pulsed loads. Planned future development of the battery model includes accurate thermal model to provide insight as to whether the ability of the li-ion NMC battery system to facilitate the LDEW load dynamics is limited by the cell and system thermal behavior.

Author Contributions: This work was carried out in collaboration between all authors. Author L.F. proposed and developed the study concept, system models, carried out model validation, data analysis, investigation and wrote this paper. Author R.B. reviewed and provided supervision for this work and this paper. All authors have read and agreed to the published version of the manuscript.

Funding: This research received no external funding.

Acknowledgments: This paper is based in part on work undertaken by Luke Farrier in part fulfilment of his PhD in the Marine Research Group at University College London. The authors would like to thank Professor Cat Savage from Defence Equipment and Support for co-supervising this PhD research. The authors would also like to thank Corvus Energy Ltd. for their support in this research and Konrad Yearwod for reviewing the paper.

Conflicts of Interest: The authors declare no conflict of interest.

References

1. Mills, K.; Xiong, J.; Liu, X.; Venkatesh, P. Informing the power system performance envelope for pulse load operation. In *Proceedings of the International Naval Engineering Conference, Glasgow, UK, 2–4 October 2018*; IMarEST: Glasgow, UK, 2018.

2. Gattozzi, A.L.; Herbst, J.D.; Hebner, R.E.; Blau, J.A.; Cohn, K.R.; Colson, W.B.; Sylvester, J.E.; Woehrman, M.A. Power system and energy storage models for laser integration on naval platforms. In Proceedings of the 2015 EEE Electric Ship Technologies Symposium (ESTS 2015), Washington, DC, USA, 21–24 June 2015; pp. 173–180.
3. O'Rourke, R. Navy Shipboard Lasers for Surface, Air, and Missile Defense: Background and Issues for Congress. Available online: https://fas.org/sgp/crs/weapons/R41526.pdf (accessed on 12 March 2020).
4. Doerry, N.; Amy, J.; Krolick, C. History and the Status of Electric Ship Propulsion, Integrated Power Systems, and Future Trends in the U.S. Navy. *Proc. IEEE* **2015**, *103*, 2243–2251. [CrossRef]
5. McCoy, T.J. Integrated Power Systems—An Outline of Requirements and Functionalities for Ships. *Proc. IEEE* **2015**, *103*, 2276–2284. [CrossRef]
6. O'Rourke, R. *Navy Lasers, Railgun, and Gun-Launched Guided Projectile: Background and Issues for Congress*; Congressional Research Service: Washington, DC, USA, 2018.
7. Petersen, L.J.; Ziv, M.; Burns, D.P.; Dinh, T.Q.; Malek, P.E. U.S. Navy efforts towards development of future naval weapons and integration into an All Electric Warship (AEW). In Proceedings of the Engine as a Weapon IV, London UK, 12–13 September 2011.
8. Wetz, D.A.; Novak, P.M.; Shrestha, B.; Heinzel, J.; Donahue, S.T. Electrochemical Energy Storage Devices in Pulsed Power. *IEEE Trans. Plasma Sci.* **2014**, *42*, 3034–3042. [CrossRef]
9. Markle, S. *Presentation: U.S. Surface Navy Electrical Leap Forward … … .a Vision for the Future*; Naval Postgraduate School: Washington, DC, USA, 2018.
10. Huhman, B.M.; Wetz, D.A.; Mili, L. Development of a Rep-Rated Pulsed Power System Utilizing Electrochemical Prime Power. *IEEE Trans. Plasma Sci.* **2016**, *44*, 3398–3408. [CrossRef]
11. Langston, J.; Steurer, M.; Bosworth, M.; Soto, D.; Longo, D.; Uva, M.; Carlton, J. Power Hardware-in-the-Loop Simulation Testing of a 200 MJ Battery-Based Energy Magazine for Shipboard Applications. In Proceedings of the 2019 IEEE Electric Ship Technologies Symposium, Arlington, VA, USA, 14–16 August 2019; pp. 39–44.
12. Farrier, L.; Savage, C.; Bucknall, R. Simulating Pulsed Power Load Compensation using Lithium-ion Battery Systems. In Proceedings of the 2019 IEEE Electric Ship Technologies Symposium (ESTS), Arlington, VA, USA, 14–16 August 2019; pp. 45–51.
13. Farrier, L.; Bucknall, R. Assessing battery energy storage for integration with hybrid propulsion and high energy weapons. In *Proceedings of the Engine as a Weapon VII, London, UK, 2–3 June 2019*; IMarEST: London, UK, 2019.
14. IEEE Recommended Practice for 1 kV to 35 kV Medium-Voltage DC Power Systems on Ships. In *IEEE Std 1709-2018 (Revision IEEE Std 1709-2010)*; IEEE: Piscataway, NJ, USA, 2018; pp. 1–54.
15. Moran, S. *The Basics of Electric Weapons and Pulsed-Power Technologies*; Naval Surface Warfare Centre: Dahlgren, VA, USA, 2012.
16. McAulay, A.D. *Military Laser Technology for Defense*, 1st ed.; John Wiley & Sons, Inc.: Hoboken, NJ, USA, 2011; ISBN 9780470255605.
17. Katz, J.; Margalit, S.; Harder, C.; Wilt, D.; Yariv, A. The Intrinsic Electrical Equivalent Circuit of a Laser Diode. *IEEE J. Quantum Electron.* **1981**, *17*, 4–7. [CrossRef]
18. Hentunen, A.; Lehmuspelto, T.; Suomela, J. Time-domain parameter extraction method for Thevenin-equivalent circuit battery models. *IEEE Trans. Energy Convers.* **2014**, *29*, 558–566. [CrossRef]
19. Cheng, X.; Yao, L.; Xing, Y.; Pecht, M. Novel Parametric Circuit Modeling for Li-Ion Batteries. *Energies* **2016**, *9*, 539. [CrossRef]
20. Nikolian, A.; Firouz, Y.; Gopalakrishnan, R.; Timmermans, J.M.; Omar, N.; van den Bossche, P.; van Mierlo, J. Lithium ion batteries-development of advanced electrical equivalent circuit models for nickel manganese cobalt lithium-ion. *Energies* **2016**, *9*, 360. [CrossRef]
21. Roscher, M.A.; Bohlen, O.S.; Sauer, D.U. Reliable state estimation of multicell Lithium-ion battery systems. *IEEE Trans. Energy Convers.* **2011**, *26*, 737–743. [CrossRef]
22. Li, J.; Mazzola, M.S. Accurate battery pack modeling for automotive applications. *J. Power Sources* **2013**, *237*, 215–228. [CrossRef]
23. Weaver, W.W.; Robinett, R.D.; Wilson, D.G.; Matthews, R.C. Metastability of Pulse Power Loads Using the Hamiltonian Surface Shaping Method. *IEEE Trans. Energy Convers.* **2017**, *32*, 820–828. [CrossRef]
24. Saad, A.A.; Faddel, S.; Youssef, T.; Mohammed, O. Small-signal model predictive control based resilient energy storage management strategy for all electric ship MVDC voltage stabilization. *J. Energy Storage* **2019**, *21*, 370–382. [CrossRef]

25. Titterton, D.H. *Military Laser Technology and Systems*; Artech House: Norwood, MA, USA, 2015; ISBN 1608077799.
26. Kasicheyanula, S.; John, V. Adaptive Control Strategy for Ultracapacitor Based Bidirectional DC–DC Converters. *IEEE Trans. Ind. Appl.* **2019**, *55*, 1717–1728. [CrossRef]
27. Birkl, C.R.; Roberts, M.R.; McTurk, E.; Bruce, P.G.; Howey, D.A. Degradation diagnostics for lithium ion cells. *J. Power Sources* **2017**, *341*, 373–386. [CrossRef]
28. Wetz, D.A.; Shrestha, B.; Donahue, S.T.; Wong, D.N.; Martin, M.J.; Heinzel, J. Capacity fade of 26650 lithium-ion phosphate batteries considered for use within a pulsed-power system's prime power supply. *IEEE Trans. Plasma Sci.* **2015**, *147*, 1448–1455. [CrossRef]
29. Liu, Y.; Zhu, Y.; Cui, Y. Challenges and opportunities towards fast-charging battery materials. *Nat. Energy* **2019**, *4*, 540–550. [CrossRef]
30. Takami, N.; Ise, K.; Harada, Y.; Iwasaki, T.; Kishi, T.; Hoshina, K. High-energy, fast-charging, long-life lithium-ion batteries using TiNb2O7anodes for automotive applications. *J. Power Sources* **2018**, *396*, 429–436. [CrossRef]
31. De Hoog, J.; Timmermans, J.M.; Ioan-Stroe, D.; Swierczynski, M.; Jaguemont, J.; Goutam, S.; Omar, N.; Van Mierlo, J.; Van Den Bossche, P. Combined cycling and calendar capacity fade modeling of a Nickel-Manganese-Cobalt Oxide Cell with real-life profile validation. *Appl. Energy* **2017**, *200*, 47–61. [CrossRef]
32. De Hoog, J.; Jaguemont, J.; Nikolian, A.; Van Mierlo, J.; Van Den Bossche, P.; Omar, N. A combined thermo-electric resistance degradation model for nickel manganese cobalt oxide based lithium-ion cells. *Appl. Therm. Eng.* **2018**, *135*, 54–65. [CrossRef]